J Neurophysiol 117: 163–177, 2017.
First published October 19, 2016; doi:10.1152/jn.00415.2016.

RESEARCH ARTICLE | *Neural Circuits*

Thalamic state control of cortical paired-pulse dynamics

Clarissa J. Whitmire, Daniel C. Millard, and Garrett B. Stanley
Wallace H. Coulter Department of Biomedical Engineering, Georgia Institute of Technology and Emory University, Atlanta, Georgia

Submitted 26 May 2016; accepted in final form 15 October 2016

Whitmire CJ, Millard DC, Stanley GB. Thalamic state control of cortical paired-pulse dynamics. *J Neurophysiol* 117: 163–177, 2017. First published October 19, 2016; doi:10.1152/jn.00415.2016.—Sensory stimulation drives complex interactions across neural circuits as information is encoded and then transmitted from one brain region to the next. In the highly interconnected thalamocortical circuit, these complex interactions elicit repeatable neural dynamics in response to temporal patterns of stimuli that provide insight into the circuit properties that generated them. Here, using a combination of in vivo voltage-sensitive dye (VSD) imaging of cortex, single-unit recording in thalamus, and optogenetics to manipulate thalamic state in the rodent vibrissa pathway, we probed the thalamocortical circuit with simple temporal patterns of stimuli delivered either to the whiskers on the face (sensory stimulation) or to the thalamus directly via electrical or optogenetic inputs (artificial stimulation). VSD imaging of cortex in response to whisker stimulation revealed classical suppressive dynamics, while artificial stimulation of thalamus produced an additional facilitation dynamic in cortex not observed with sensory stimulation. Thalamic neurons showed enhanced bursting activity in response to artificial stimulation, suggesting that bursting dynamics may underlie the facilitation mechanism we observed in cortex. To test this experimentally, we directly depolarized the thalamus, using optogenetic modulation of the firing activity to shift from a burst to a tonic mode. In the optogenetically depolarized thalamic state, the cortical facilitation dynamic was completely abolished. Together, the results obtained here from simple probes suggest that thalamic state, and ultimately thalamic bursting, may play a key role in shaping more complex stimulus-evoked dynamics in the thalamocortical pathway.

NEW & NOTEWORTHY For the first time, we have been able to utilize optogenetic modulation of thalamic firing modes combined with optical imaging of cortex in the rat vibrissa system to directly test the role of thalamic state in shaping cortical response properties.

cortical activation; dynamics; optogenetics; thalamic state; vibrissa

SENSORY PATHWAYS are strongly influenced by the interplay between excitation and inhibition that carves out complex neural dynamics. Stimulus-evoked dynamics are highly sensitive both to timing of patterns of sensory stimulation on slower timescales of hundreds of milliseconds and to timing of synaptic inputs on faster timescales of tens of milliseconds. However, because of the complexity of the neural circuitry, the relevant mechanisms are still unclear. Nonlinear dynamics in the thalamocortical circuit have been investigated in vision and audition (Hawken et al. 1990; Kilgard and Merzenich 1998) but are particularly well studied in the rodent vibrissa system (Boloori et al. 2010; Boloori and Stanley 2006; Castro-Alamancos and Connors 1996a; Civillico and Contreras 2005; Higley and Contreras 2007; Simons 1985). Paradoxically, the nonlinear dynamics of the circuit have been characterized as both suppressive and facilitative in a range of experimental conditions because of complexities in the temporal interactions between excitatory and inhibitory network dynamics (Ego-Stengel et al. 2005; Webber and Stanley 2004, 2006). However, because previous studies used only peripheral sensory stimulation of the whiskers to study the dynamics of the pathway, it has not yet been possible to disambiguate dynamics due to prethalamic effects from those established in the thalamocortical circuit.

Because of unique cellular and circuit properties, the thalamus is ideally positioned to dynamically gate and/or modulate information transmission to cortex (Crick 1984). Specifically, the thalamus operates in two distinct firing modes: tonic firing and burst firing (Sherman 2001). Switching between these two states occurs regularly in concert with shifts in arousal (Fanselow et al. 2001; Llinas and Steriade 2006; Ramcharan et al. 2000), attention (McAlonan et al. 2008), or sensory drive (Whitmire et al. 2016) and is linked through these mechanisms to the desynchronized thalamocortical state (Crochet and Petersen 2006; Poulet and Petersen 2008). Through the use of optogenetics, recent work has demonstrated that the artificial hyperpolarization or depolarization of the thalamus is sufficient to drive cortex into the synchronized (Halassa et al. 2011) or desynchronized (Poulet et al. 2012) state, and yet the effect of thalamic state on the propagation of stimulus-evoked activity to downstream structures remains poorly understood.

Here, using simple stimulus probes, we experimentally investigated the thalamocortical circuit of the rodent vibrissa pathway in response to whisker, electrical, and optogenetic inputs, using voltage-sensitive dye (VSD) imaging (VSDI) to record the spatiotemporal stimulus-evoked cortical activity. Specifically, the VSDI targeted subthreshold activity in the supragranular layers of cortex (layer 2/3), reflecting suprathreshold input from cortical layer 4 (Wang et al. 2012; Zheng et al. 2015). Consistent with previous literature, we found that simple whisker deflections primarily produced suppression for all stimulus intensities. In contrast, artificial thalamic stimuli elicited significant cortical facilitation. We hypothesized that this facilitation could be due to the bursting dynamics between the thalamocortical projection nucleus [ventroposterior medial nucleus (VPm)] and the inhibitory reticular nucleus (nRT) of

Address for reprint requests and other correspondence: G. B. Stanley, Coulter Dept. of Biomedical Engineering, Georgia Inst. of Technology and Emory Univ., 313 Ferst Dr., Atlanta, GA 30332 (e-mail: garrett.stanley@bme.gatech.edu).

the thalamus. To determine the effect of thalamic state, or thalamic polarization levels, on the facilitation, we used direct optogenetic control of thalamic depolarization to shift the thalamic firing patterns from burst to tonic encoding. The removal of bursting through optogenetic modulation of thalamic state eliminated the cortical facilitation elicited by subthreshold thalamic microstimulation, such that the dynamics were purely suppressive and therefore more similar to those of actual sensory stimuli. In light of these findings, we suggest that the interplay between excitation and inhibition in the thalamocortical circuit, in concert with burst/tonic state regulation in thalamus, shapes the signaling in the pathway and may serve to enhance specific temporal patterns of sensory inputs.

METHODS

Experimental preparation. All procedures were approved by the Institutional Animal Care and Use Committee at the Georgia Institute of Technology and were in agreement with guidelines established by the National Institutes of Health. Eighteen adult female albino rats (220–350 g, Sprague-Dawley; Charles River Laboratories, Wilmington, MA) were used in the study. Briefly, female albino rats were sedated with 2% vaporized isoflurane and anesthetized with pentobarbital sodium (50 mg/kg ip, initial dose); supplemental doses were given as needed to maintain a surgical level of anesthesia, confirmed by measurements of heart rate, respiration, and eyelid/pedal reflexes to averse stimuli (toe or tail pinch). Importantly, only physiological measurements were used to maintain the anesthesia level. Simultaneous electrophysiological measurements of cortical activity were not performed within this study. Therefore, there are no electrical measures of cortical state such as local field potential to quantify the anesthesia depth from a neurological perspective. In all experiments, body temperature was maintained at 37°C by a servo-controlled heating blanket (FHC, Bowdoinham, ME). After initial anesthesia, the animal was mounted on a stereotactic device (Kopf Instruments, Tujunga, CA) in preparation for the surgery and subsequent recordings. Atropine (0.5 mg/kg sc) was injected and lidocaine was administered subdermally to the scalp. After the initial midline incision on the head, tissue and skin were resected and connective tissue was carefully removed. A craniotomy was made on the left hemisphere over the barrel cortex (stereotactic coordinates: 1.0–4.0 mm caudal to the bregma, 3.5–7.0 mm lateral to the midline) and over the VPm of the thalamus (2.0–4.0 mm caudal, 2.0–3.5 mm lateral to the midline; Paxinos and Watson 1998). A dam was constructed with dental acrylic around the craniotomy over the barrel cortex to contain the VSD solution (RH1691, 1.5 mg/ml; Optical Imaging, Rehovot, Israel) for staining. Mineral oil was periodically applied to the cortical surface over VPm to keep the brain moist. After the recording session, the animal was euthanized with an overdose of pentobarbital sodium.

A separate batch of experiments ($n = 5$ of 18 animals) was performed recording only the electrophysiological response of single neurons in the VPm of the thalamus to optogenetic stimulation in the thalamus. These surgical procedures were performed as described above but differed in the anesthetic used during recording [fentanyl cocktail anesthesia: fentanyl (5 μg/kg), midazolam (2 mg/kg), and dexmedetomidine (150 μg/kg)].

VSD imaging. VSDI was achieved by using a high-speed, low-noise camera coupled with a tandem lens (MiCAM 2; SciMedia, Tokyo, Japan). After the craniotomy over the barrel cortex, the dura mater was allowed to dry for 15 min (Lippert et al. 2007). The cortex was stained with a solution of dye RH1691 (1.5 mg/ml; Optical Imaging) for 2 h, during which the dye solution was circulated every 5 min to prevent the cerebrospinal fluid from impeding the staining. After staining, saline was applied generously to wash off the dye residue. The dam was then filled with saline, and a glass cover slide was placed on top of the dam to prevent the saline from vaporizing. The dye was excited by a 150-W halogen lamp filtered to pass wavelengths only in the 615–645 nm band. In all experiments, a ×1.0 magnification lens was used as the objective lens in conjunction with a ×0.63 condenser lens to provide ×1.6 magnification (48 pixels/mm). Twenty trials of VSD data were collected for each stimulus, and they were averaged off-line for the data analysis (see *VSD analysis*).

VSD analysis. Multiple trials of VSDI data were collected for each stimulus. For each trial, the 40 frames (200 ms) collected before the presentation of the stimulus were averaged to calculate the background fluorescence, against which the activation was measured. For each frame, the background fluorescence was subtracted to produce a differential signal ΔF. Additionally, each frame was divided by the background image to normalize for uneven illumination and staining to produce the signal $\Delta F/F_0$. For presentation purposes only, the individual trials were averaged together and then filtered with a 9 × 9 pixel (~200 × 200 μm) spatial averaging filter. The anatomical mapping, acquired through cytochrome oxidase histology, was registered with the functional cortical column mapping from VSDI by solving a linear inverse problem, the details of which have been described previously (Wang et al. 2012). After the functional image registration, the cortical response was discretized, where each signal corresponds to a single functional cortical column. In so doing, the VSDI signal was averaged spatially within the contour of the cortical column.

The cortical response amplitude (R) was quantified as the maximum VSDI signal elicited in response to each stimulus in the paired-pulse paradigm, after averaging within a single cortical column, on a trial-by-trial basis. The paired-pulse ratio (PPR) was defined as the response to the second stimulus (R2) divided by the sum of the response to the first (R1) and second (R2) stimuli [PPR = R2/(R1 + R2)]. A simple ratio of R2/R1, as has been used previously for electrophysiology data (Jouhanneau et al. 2015), was not used here for imaging data because near-zero changes in the fluorescence in response to the first stimulus would push the ratio toward infinity. In this work, a PPR of 0.5 corresponds to no interaction between the pair of stimuli, as they elicited equal responses to the first and second stimuli, assuming the response to the first stimulus had completely decayed before the onset of the response to the second stimulus. A PPR of <0.5 means that the response to the second stimulus was smaller than the response to the first (suppression), while a PPR of >0.5 corresponds to a larger response to the second stimulus (facilitation).

The time course of the VSD signal decay was quantified in response to the first stimulus in the pair. Each trial was only characterized if the peak evoked response was greater than three times the standard deviation of the background fluctuation (as quantified from the 200-ms VSD trace before stimulus onset). The VSD signal from the peak evoked response to 125 ms afterwards (25 frames) was used to fit a sum of exponentials where

$$\mathrm{VSD} = a_1 e^{-t/\tau_1} + a_2 e^{-t/\tau_2}$$

τ_1 was restricted to be the shorter time constant, while τ_2 was the longer time constant.

Electrophysiological recordings. Extracellular recordings in the VPm were obtained by using single tungsten microelectrodes (~1 MΩ, 75 μm in diameter; FHC). The procedure was described in detail previously (Wang et al. 2010). Briefly, after the craniotomy a tungsten microelectrode was slowly advanced into VPm with a hydraulic micropositioner (Kopf Instruments). During electrode advancement through VPm, individual whiskers were stimulated manually to identify the principal whisker, i.e., the whisker that evokes the strongest response. We aimed to recruit barrel fields in the E and D rows, which are located close to the center of the imaging field in our preparation. Neuronal signals were amplified, band-pass filtered (500 Hz–5 kHz), digitized at 30 kHz/channel, and collected with a 32-, 64-, or 96-channel data-acquisition system (Plexon, Dallas, TX; Blackrock Microsytems, Salt Lake city, UT; and Tucker Davis Technologies,

Alachua, FL, respectively). Data were then sorted with WaveClus software (Quiroga et al. 2004). Data were excluded if the neuron was not light sensitive (<1 spike/stimulus at the strongest light intensity) or if the waveform was not sufficiently isolated [as quantified by the waveform signal-to-noise ratio (SNR)]. Waveform SNR was defined as the peak-to-peak voltage of the mean waveform divided by the average standard deviation of the waveform over the full waveform snippet for all recorded waveforms. All cells with a waveform SNR < 3 were excluded from the analysis.

Electrophysiological analysis. Single-unit thalamic responses were recorded in response to optogenetic stimulation with a custom optrode consisting of an optical fiber (200-μm diameter; Thorlabs, Newton, NJ) and an electrode (tungsten microelectrode; FHC) that was lowered into the VPm. The response to the stimulus was quantified as the number of spikes in 20 ms following the onset of the light pulse. Spikes were classified as part of a T-type calcium channel burst if two or more spikes were separated by an interspike interval of 4 ms or less and the first spike in the burst was preceded by at least 100 ms of silence (Lesica et al. 2006; Lu et al. 1992; Reinagel et al. 1999). The burst ratio was defined as the number of burst spikes within the 20-ms response window divided by the total number of spikes within the 20-ms response window, as described previously (Whitmire et al. 2016). The first spike latency was defined as the first spike following stimulus onset. Any latencies > 5 ms were excluded from the trial average, as this indicated the lack of a light-evoked response.

Thalamic microstimulation. After the principal whisker was identified, the thalamic electrode was used to deliver single electrical current pulses to evoke cortical responses in the somatosensory pathway. The electrical stimuli were created with a digital stimulus generator (model DS8000; WPI, Sarasota, FL) and delivered with a digital linear stimulus isolator (model DLS 100; WPI) acting in current source mode. All individual electrical stimuli were charge-balanced, cathode-leading, symmetrical biphasic current pulses of 200-μs duration per phase. A paired-pulse stimulus paradigm was used, in which two stimuli with the same current amplitude were delivered separated by an interstimulus interval (ISI). Current amplitudes (30–150 μA) and ISIs (50, 100, 150, 200, 250, 500 ms) were varied. Current amplitudes were chosen to span the full range of cortical activation from no response to maximal cortical excitation.

Whisker stimulation. Sensory stimulation was applied through computer-controlled whisker deflections. Whiskers were trimmed at ~12 mm from the face and were inserted into a glass pipette fixed to the end of a calibrated multilayered piezoelectric bimorph bending actuator [range of motion 1 mm, bandwidth 200 Hz; Physik Instrumente (PI), Auburn, MA] positioned 10 mm from the vibrissa pad. Vibrissae were always deflected in the rostral-caudal plane. Punctate deflections consisting of exponential rising and falling phases (99% rise time, 5 ms; 99% fall time, 5 ms) were used as sensory stimuli (Boloori et al. 2010; Wang et al. 2010). A paired-pulse stimulus paradigm was used, in which two whisker stimuli with the same velocity were delivered separated by a specified ISI. Velocities (75–1,200°/s) and ISIs (50, 100, 150, 200, 250, 500 ms) were varied. Whisker velocities were chosen to span the full range of cortical activation from no response to maximal cortical excitation.

Optogenetic expression. A subset of animals ($n = 7$) underwent an initial surgery for the injection of a viral vector (UNC Vector Core, Chapel Hill, NC) to induce expression of either channelrhodopsin [ChR2; AAV-CaMKIIa-hChR2(H134R)-mCherry] or the stabilized step function opsin [SSFO; AAV-CaMKIIa-hChR2(C128S/D156A)-mCherry]. The viral injection (1 μl) was delivered at a rate of 0.2 μl/min in the VPm of the thalamus according to the coordinates described above. Given the dense structure of thalamus, expression was restricted to excitatory neurons by using the CaMKIIa promoter (Aravanis et al. 2007) to prevent opsin expression in the nearby reticular thalamus (nRT). However, because of the close proximity of posteromedial thalamus (POm), it is possible that both VPm and POm expressed opsins. Viral expression was verified experimentally in all animals through light-responsive electrophysiological recordings and by histology in animals not used for experimentation. A single experimental animal was perfused for histological analysis after recording and is included in Fig. 5. Although this animal and our histology-only animals (data not shown) demonstrate strong opsin expression within the thalamus, we are not able to differentiate between VPm and POm expression within each of the experimental animals presented here.

Optical stimulation. Depolarizing opsins were used in two distinct ways: first, to drive the pathway with pairs of light pulses and second, to modulate the pathway with low-amplitude ongoing light stimulation. For both driving and modulating neural activity, light-emitting diodes (LEDs) were used to excite the ChR2 and SSFO in vivo. An "optrode" was positioned in the VPM thalamus, with the fiber optic directly attached to the LED to minimize light loss. A 465-nm LED was used for animals expressing ChR2. When driving the pathway, the same paired-stimulus design implemented for sensory and electrical stimulation was used for optical stimulation. Two 5-ms pulses of light at varying intensity (47–139 mW/mm^2) were administered with a 150-ms ISI. Light intensities were chosen to span the full range of cortical activation from no response to maximal cortical excitation. The 150-ms ISI was chosen because it most reliably activated the facilitation described for the electrical stimulation. In the thalamic electrophysiology experiments, a 470-nm LED and a commercial LED driver were used (Thorlabs).

When modulating the pathway, both ChR2 and SSFO were used. Because ChR2 quickly closed when the light was removed (Mattis et al. 2012), when this opsin was used the light was delivered continuously to maintain the long-timescale depolarization involved in this study. A custom current source was used to drive the LED (Newman et al. 2015). For animals expressing the SSFO, a 465-nm LED (LED Engin, San Jose, CA) was used in combination with a 590-nm LED (LED Engin) through a wavelength combiner (Doric Lenses, Quebec, QC, Canada). The SSFO channel has a long closing time, such that the channel remains open long past the duration of the light stimulus, so brief pulses of light (~5–50 ms) from the 465-nm LED were used to open the channel over long timescales. To close the channel, 15 s of yellow light from the 590-nm LED was delivered through the fiber optic. SSFO and ChR2 were activated in conjunction with electrical stimulation (paired-pulse design as described above) in VPm to assess the effects of thalamic state on cortical activation.

Statistical analysis. The statistical analyses performed in this study were implemented with multiway ANOVA (factors included animal, stimulus condition, and stimulus number). For the PPR, an assumption of normality is violated by the data bounds of 0 and 1, which would limit the accuracy of the ANOVA. To overcome this limitation, the PPR data were transformed from bounded data ([0,1]) to unbounded data ($[-\infty,\infty]$) with a logit function and statistical significance was assessed with respect to the first stimulus condition. All statistical tests of partially bounded data, such as spike counts, were performed on the original data without any transformation.

RESULTS

Artificial stimulation of thalamus isolates dynamics of thalamocortical processing. In this work, we experimentally investigated the simple dynamics of the thalamocortical circuit of the rodent vibrissa somatosensory system (Fig. 1*A*). Specifically, we utilized paired-pulse inputs (Fig. 1*B*), where the spatiotemporal cortical activation was measured in response to temporally spaced pairs of whisker, electrical, and optogenetic inputs with VSDI (Fig. 1*C*). In a subset of experiments, thalamic state was modulated optically in conjunction with microstimulation of thalamus to investigate the role of thalamic state on information transmission (Fig. 1*B*, *bottom*). The temporal component of the cortical response was extracted from

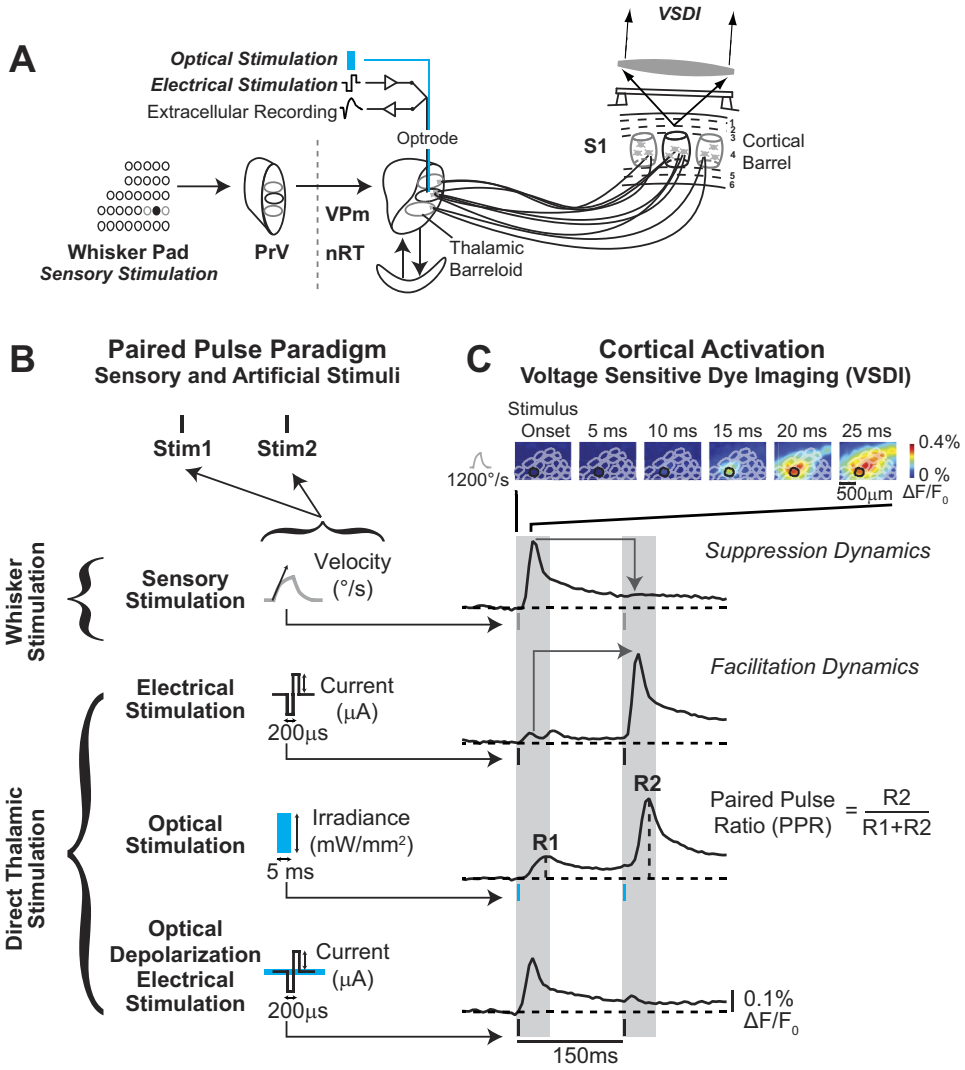

Fig. 1. Quantification of thalamocortical dynamics using natural and artificial paired-pulse paradigm. *A*: schematic of the feedforward lemniscal circuit of the rat whisker pathway from the whisker pad to the brain stem principal nucleus (PrV) of the trigeminal complex, the ventral posteromedial (VPm) nucleus of the thalamus, and ultimately primary somatosensory cortex (S1). The optrode was positioned in the VPm for optical and electrical stimulation. VSDI, voltage-sensitive dye imaging. *B*: the paired-pulse paradigm consists of 2 temporally spaced stimuli administered at the whisker (sensory stimulus) or directly to the thalamus (electrical and optical stimulation). *C*: VSDI of the barrel cortex recorded the cortical activation (*top*). The activity within a barrel/region of interest is averaged together to quantify the temporal response to a stimulus (black traces). Trial-averaged examples of the cortical response are depicted in response to pairs of whisker (1,200°/s), electrical (40 μA), optical (90 mW/mm^2), and electrical in the presence of optical depolarization (60 μA) stimuli.

the full spatiotemporal images by computing the mean activity within a specific barrel in each frame (Fig. 1*C*, *top*; region of interest outlined in black), and the response was computed as the maximum amplitude of the evoked response in a window following stimulus presentation relative to baseline (Fig. 1*C*, optical stimulation, R1, R2). The dynamics of the cortical response were classified as suppressive when the response to the first stimulus was larger than the response to the second (Fig. 1, sensory stimulation, 1,200°/s) and facilitative when the response to the first stimulus was smaller than the response to the second (Fig. 1, electrical stimulation, 40 μA). Furthermore, while whisker stimulation will activate each stage of the sensory pathway, the artificial stimulation through electrical and optogenetic means will circumvent prethalamic processing by directly activating the thalamocortical relay neurons, providing a mechanism to separate the dynamics of the thalamocortical circuit from the processing that occurs from the periphery to thalamus (Fig. 1*A*; see DISCUSSION for additional information about artificial stimulation of thalamus).

Sensory stimulation elicits primarily suppression dynamics. Temporal patterns of sensory input are known to produce nonlinear responses even in the early sensory pathways (Chung et al. 2002; Ganmor et al. 2010). Significant work from the thalamocortical circuit of the rodent whisker system, using pairs or triplets of individual whisker deflections to map out the dynamics of neurons in the primary somatosensory cortex, has principally detailed paired-pulse suppression, where the response to the second stimulus is suppressed because of the presence of a previous stimulus occurring immediately prior (Boloori et al. 2010; Boloori and Stanley 2006; Castro-Alamancos and Connors 1996a; Simons 1985; Webber and Stanley 2004, 2006), which can lead to more complex dynamics in response to richer patterns of inputs. Here, in agreement with these studies, we used pairs of whisker stimuli at varying ISIs with fixed stimulus intensities (Fig. 2*A*, *top*; velocity = 150, 1,200°/s) and varying velocities with a fixed ISI (Fig. 2*B*, *top*; ISI = 150 ms) to directly probe the second-order dynamics of the system. Figure 2*A* shows an example of the temporal response in cortex, averaged across trials, to pairs of whisker deflections at low (Fig. 2*A*, *left*) and high (Fig. 2*A*, *right*) angular velocities. When the whisker stimulus was weak, the response to the second stimulus was approximately equal in strength to the response to the first stimulus, except at the 50-ms ISI (Fig. 2*A*, *left*), indicating a very short duration for the dynamic interactions between the responses to the deflections in the sequence. However, when the whisker stimulus

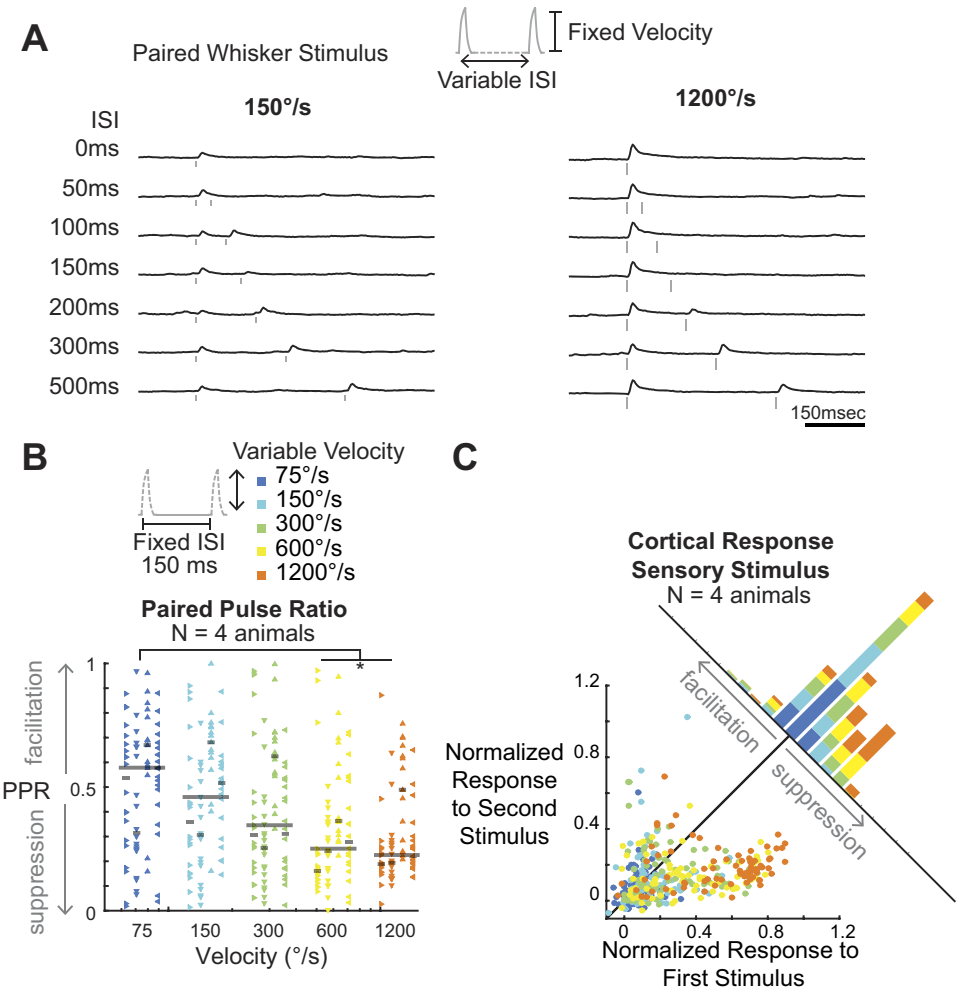

Fig. 2. Sensory-evoked cortical dynamics elicit suppressive paired-pulse dynamics. *A*, *left*: cortical response to pairs of weak (150°/s) whisker stimuli. The response to the second stimulus was suppressed only for the 50-ms interstimulus interval (ISI). *Right*: cortical response to pairs of high-velocity (1,200°/s) whisker deflections at varying ISI. The response to the second stimulus was suppressed relative to the first, with the suppression relaxing for longer ISIs. *B*, *top*: with the ISI fixed at 150 ms, the velocity of the stimuli was varied systematically. *Bottom*: the paired-pulse ratio (PPR) is plotted as a function of stimulus intensity, represented by color. Each trial across experiments (n = 4 animals, each denoted by a vertical line of points) is plotted as a dot, with the median of the distribution indicated by the horizontal black bars (animal median shown as well as population median). For each condition, asterisk indicates statistical significance relative to first stimulus condition (2-way ANOVA; factors: animal, stimulus condition; $P < 0.05$). P values for each stimulus condition [150, 300, 600, 1,200°/s] relative to the first stimulus condition (75°/s) are P = [0.8727, 0.2698, 3.73e-4, 3.99e-5]. *C*: the normalized response to the first and second stimuli are plotted for all single trials across all whisker deflection velocities at the 150-ms ISI for all experiments (n = 4 animals). Along the diagonal, a histogram represents the distance of each trial from the unity line (black). Data below the unity line are indicative of suppressive dynamics, while data above the unity line are indicative of facilitation dynamics.

was strong, the cortical response exhibited profound paired-pulse suppression (Fig. 2*A*, *right*) such that the response to the second stimulus was strongly suppressed relative to the first. This suggests an activity-dependent modulation of the dynamics, consistent with previous reports in the barrel cortex (Boloori et al. 2010). To quantify the strength of the suppression as a function of stimulus intensities, we analyzed single trials of the VSDI signal for the fixed 150-ms ISI across velocities (Fig. 2*B*, *top*). The response to each stimulus was defined as the peak cortical response in the window after stimulus onset relative to the baseline activity level before any stimulation. Note that the cortical activity after the first stimulus may not have returned to baseline before the onset of the second stimulus (see Fig. 4). Rather than making any assumptions about the interaction between the ongoing cortical activity and the second stimulus-evoked response, we used absolute maximum fluorescence values. The dynamics of the evoked response were quantified with a PPR [Fig. 1*B*; PPR = R2/(R2 + R1), see METHODS for additional details]. With this metric, a value > 0.5 is indicative of facilitation dynamics and a value < 0.5 is indicative of suppression dynamics. The PPR is <0.5 for stronger whisker velocities, indicative of stronger paired-pulse suppression with stronger stimuli (Fig. 2*B*, *bottom*; n = 4 animals; 2-way ANOVA).

On a single-trial basis, the peak response to the second stimulus was plotted relative to the peak response to the first stimulus (Fig. 2*C*). Each data point is the peak cortical response to a single presentation of the paired-pulse stimulus, with the color indicating the velocity of the whisker deflections. As the velocity of the whisker deflections increased, the response to the first stimulus also increased. However, for all velocities, the response to the second stimulus was suppressed relative to the first for the majority of trials, as most of the data points fell below the unity line (Fig. 2*C*, black). These trends are consistent across four experiments, where the data from each experiment have been normalized (Fig. 2*C*). A few trials at low velocity showed strong responses to the second stimulus with no response to the first, but this occurred at low probability. This is consistent with the response to the second stimulus being dependent on the first and responding probabilistically in the same manner as the first response (Gollnick et al. 2016). We can estimate the amount of suppression or facilitation on each trial by computing the distance from the unity line for each trial (Fig. 2*C*, diagonal histogram). This depiction shows that the lower stimulus intensities show very little dynamic interaction (blue data, Fig. 2*C* histogram) but as the intensity of the whisker stimulus increases the intensity of the suppression also increases (orange data, Fig. 2*C* histogram). Again, the majority of trials lie in bins below the unity

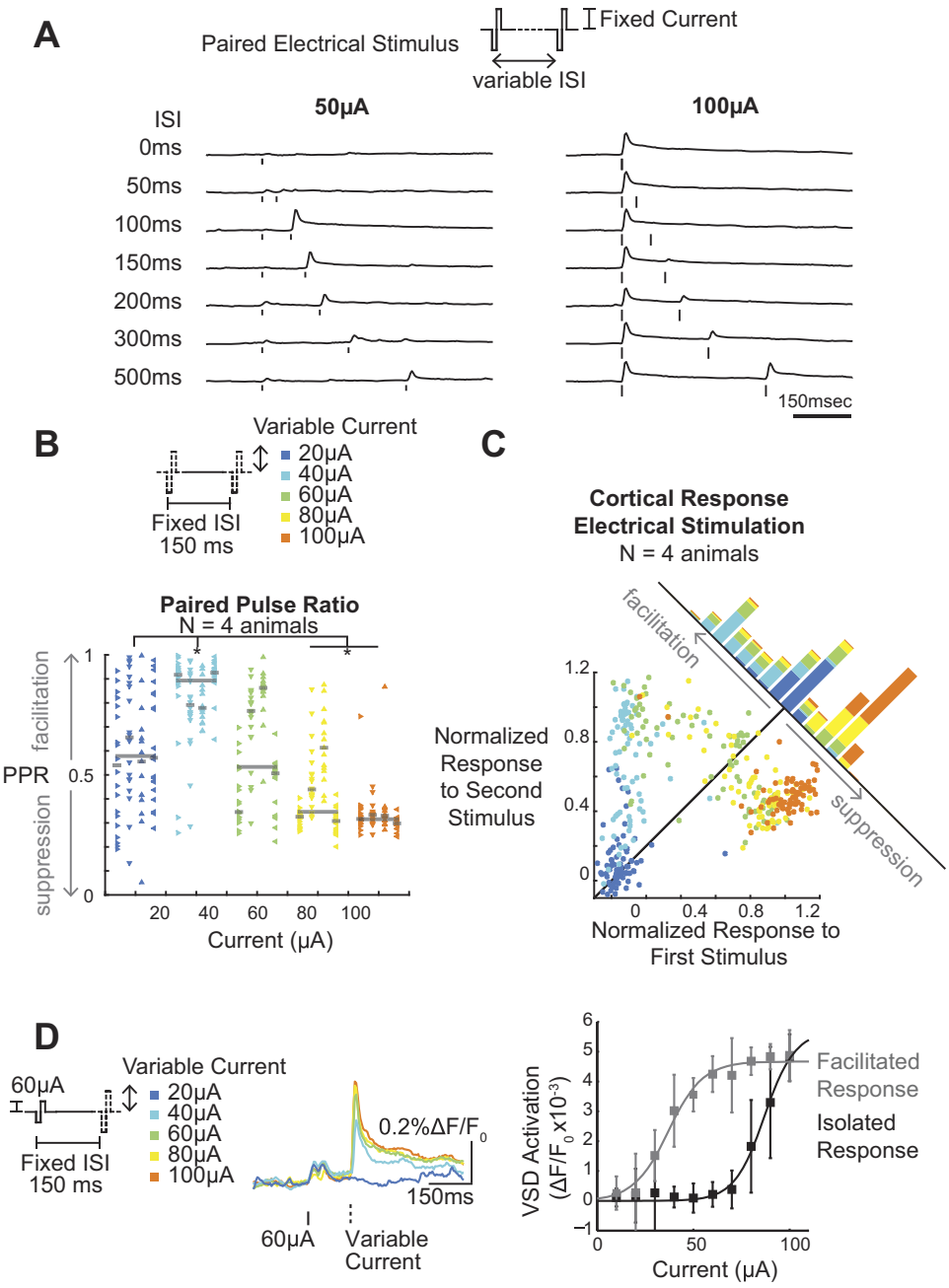

Fig. 3. Artificially evoked cortical responses elicit different paired-pulse dynamics. *A*, *left*: cortical response to pairs of weak (50 μA) electrical stimuli. The response to the second stimulus was facilitated relative to the first, but only for the 100- to 200-ms interstimulus intervals (ISIs). *Right*: cortical response to pairs of strong (100 μA) electrical stimuli at varying ISI was purely suppressive. The response to the second stimulus was suppressed relative to the first, with the suppression relaxing for longer ISIs. *B*, *top*: with the ISI fixed at 150 ms, the amplitude of the current was varied systematically. *Bottom*: the paired-pulse ratio (PPR) is plotted as a function of stimulus intensity, represented by color. Each trial across experiments (n = 4 animals, each denoted by a vertical line of points) is plotted as a dot, with the median of the distribution indicated by the horizontal black bars (animal median shown as well as population median). For each condition, asterisk indicates statistical significance relative to first stimulus condition (2-way ANOVA; factors: animal, stimulus condition; $P < 0.05$). P values for each stimulus condition [40, 60, 80, 100 μA] relative to the first stimulus condition (20 μA) are P = [9.92e-9, 0.9992, 1.08e-7, 9.92e-9]. *C*: normalized responses to the first and second stimuli are plotted for all single trials across all current amplitudes at the 150-ms ISI for all experiments (n = 4 animals). Along the diagonal, a histogram represents the distance of each trial from the unity line (black). Data below the unity line are indicative of suppressive dynamics, while data above the unity line are indicative of facilitation dynamics. Note the significant number of trials classified as facilitative. *D*, *left*: in a separate experiment (n = 1 animal), the first stimulus was held fixed at a facilitating current amplitude (60 μA) while the second stimulus was allowed to vary in amplitude. *Right*: the evoked response to the second variable amplitude stimulus (facilitated response) was greater than the response to the same current amplitude presented in isolation (isolated response). Values shown are means ± SE (10 trials per condition).

line, indicating a prevalence of paired-pulse suppression among the cortical population in response to pairs of whisker deflections.

Artificial stimulation elicits facilitative dynamics. Within the paired-pulse paradigm, we also recorded the cortical response to pairs of thalamic microstimulation pulses to disentangle thalamic and prethalamic contributions to the cortical paired-pulse dynamics. As shown for whisker stimulation, Fig. 3*A* shows an example of the temporal response in cortex, averaged across trials, to pairs of thalamic microstimuli at low and high current amplitude with varying ISIs. While the high-current stimuli exhibited paired-pulse suppression (Fig. 3*A*, *right*) similar to high-velocity whisker deflections (Fig. 2*A*, *right*), the low-current stimuli produced a dramatically different nonlinear response (Fig. 3*A*, *left*). For ISIs of 100–200 ms, the response to the second stimulus was strongly facilitated even though the first stimulus was subthreshold and produced little to no cortical response. Similar to the sensory stimulation, the PPR is ~0.5 for low current amplitudes and is significantly reduced at high current amplitudes. However, in contrast to the whisker stimuli, the PPR shows significant facilitation at intermediate current levels (Fig. 3*B*; n = 4 animals, 2-way ANOVA).

Facilitation and suppression were consistent across trials for sub- and suprathreshold stimuli, respectively. The normalized response to the second stimulus is plotted relative to the normalized response to the first for single trials and varying current amplitude for the 150-ms ISI on a trial-by-trial basis across experiments in Fig. 3*C* (n = 4 animals; same as shown for Fig. 2*C*). For the lowest current intensity (Fig. 3*C*, dark blue), there was no response to either stimulus presentation. At a slightly higher current intensity (Fig. 3*C*, light blue), the response to the second stimulus was strongly facilitated for

each trial, leading to a cluster of points in the top left quadrant of Fig. 3*C*. Importantly, the clustering in the top left quadrant of the axes distinguished the reliable facilitation of electrical stimulation from the lack of facilitative nonlinear dynamics for subthreshold whisker inputs in Fig. 2*C*. At the highest current intensities (Fig. 3*C*, yellow and orange), the response to the second stimulus was consistently suppressed relative to the first, leading to a cluster in the bottom right quadrant. At threshold stimulus intensity (Fig. 3*C*, green), the response to the first stimulus varied significantly on a trial-to-trial basis, as shown previously (Millard et al. 2015). This transition from facilitative to suppressive dynamics with increasing stimulus amplitudes is further emphasized by visualizing the distance from the unity line as a function of stimulus intensity (Fig. 3*C*, diagonal *inset*). The consistency of the pattern across animals established the distinct bimodality of the cortical nonlinear dynamics in response to thalamic microstimulation (Millard et al. 2013) compared with sensory stimuli (data in Figs. 2 and 3 were recorded from the same experimental preparation, $n = 4$ animals total).

Finally, to further isolate the cause of the facilitative effects for intermediate current amplitudes, another experiment was conducted in which the amplitude of the first pulse was fixed at a facilitative value (60 μA) and the amplitude of the second pulse was allowed to vary (Fig. 3*D*, *left*; 1 experiment). Across trials, the response to a given current amplitude preceded by a 60-μA stimulus was compared with the response to the same current amplitude presented in isolation (isolated response, Fig. 3*D*, *right*). Across all intermediate stimulus intensities, the 60-μA stimulus provided 150 ms before the test stimulus led to an enhanced, or facilitated, response (facilitated response, Fig. 3*D*, *right*).

Temporal dynamics of decay of evoked response. Importantly, the cortical response to both artificial and sensory stimuli measured with VSDI can persist for hundreds of milliseconds. To quantify this, we fit a sum of exponential equation to the decay of the evoked response to the first stimulus (Fig. 4*A*). Across conditions, the rapid decay time constant (τ_1) was on the order of 10–15 ms (Fig. 4*B*; median τ_1 values are [20.3, 16.2, 10.5, 13.1, 9.3] ms for increasing whisker stimulus amplitudes and [14.0, 20.4, 10.1, 9.5, 10.0] ms for increasing current stimulus amplitudes). However, the slow decay time constant (τ_2) was an order of magnitude larger, reaching 110 ms for the largest whisker velocity and 320 ms for the largest current amplitude (Fig. 4*C*; median τ_2 values are [64.5, 44.6, 85.2, 74.6, 110.3] ms for increasing whisker stimulus amplitudes and [55.3, 29.4, 162.8, 177.6, 323.2] ms for increasing current stimulus amplitudes). Therefore, it was often the case that the fluorescence signal had not yet returned to baseline when the second stimulus arrived 150 ms after the first. Importantly, the prolonged fluorescence trace is not likely due to temporal artifacts from the dye. Instead, evidence from simultaneously recorded VSDI of cortex with individual intracellular recordings from layer 2/3 has shown a strong correlation between the VSD signal and the subthreshold voltage fluctuations (Petersen et al. 2003). This provides strong evidence that the prolonged VSD signal is representative of the underlying neural activity rather than sensor artifacts.

If one assumes that the cortical responses to the first and second stimuli add linearly, then we could subtract the measured cortical response to a single stimulus from the paired-pulse response to isolate the amplitude of the response to the second stimulus from the ongoing response to the first pulse. However, subtraction of the estimated response to the first stimulation would only further enhance the suppression dynamic by reducing the quantified response to the second pulse and would have no impact on the facilitation dynamic due to the near-zero response to the first pulse in facilitation conditions. Rather than assuming linear superposition of the ongoing cortical activity and the stimulus-evoked response, we defined the response to the second stimulus as the maximum of the absolute amplitude of the trace without attempting to correct for ongoing cortical activity in response to the first stimulus, to avoid unnecessarily biasing the data.

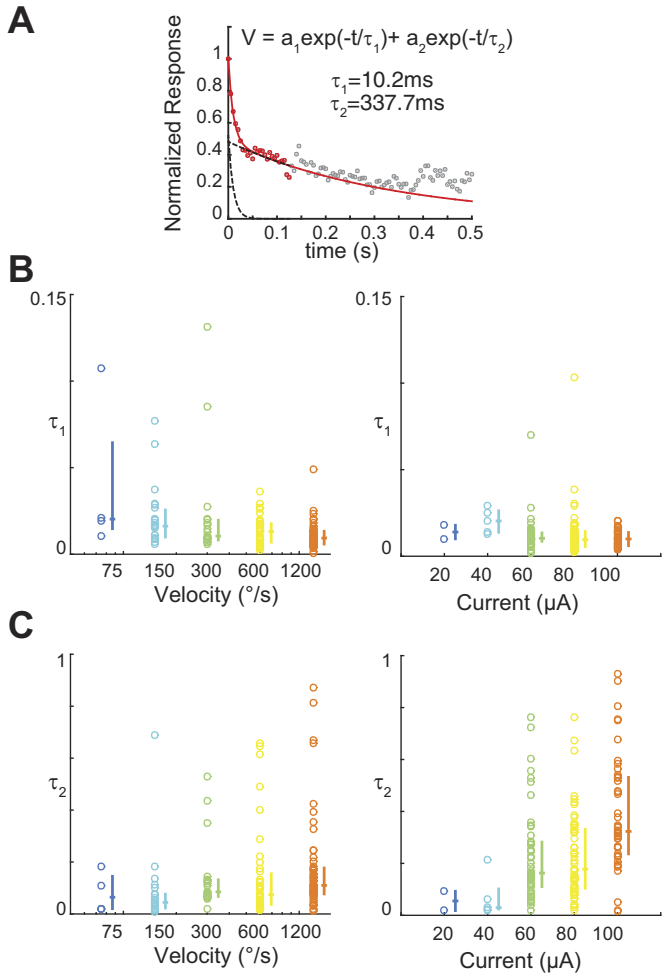

Fig. 4. Temporal dynamics of the decay of cortical activation following stimulation can last hundreds of milliseconds. *A*: the decay from the peak response was well approximated by the sum of 2 exponentials (equation, *top*). In this example (τ_1 = 10.2 ms, τ_2 = 337.7 ms), the data points used to fit the curve are shown in red while the ongoing response is shown in gray (*left*; full curve fit shown as solid red line, individual exponentials plotted as dotted lines). *B*: across experiments, τ_1 was defined as the shorter time constant. Median τ_1 values are [20.3, 16.2, 10.5, 13.1, 9.3] ms for increasing whisker stimulus amplitudes and [14.0, 20.4, 10.1, 9.5, 10.0] ms for increasing current stimulus amplitudes. *C*: across experiments, τ_2 was defined as the longer time constant. Median τ_2 values are [64.5, 44.6, 85.2, 74.6, 110.3] ms for increasing whisker stimulus amplitudes and [55.3, 29.4, 162.8, 177.6, 323.2] ms for increasing current stimulus amplitudes.

Thalamic bursting activity as mechanism underlying facilitation dynamics. In a separate set of experiments ($n = 5$ animals), we performed an identical analysis for optogenetic

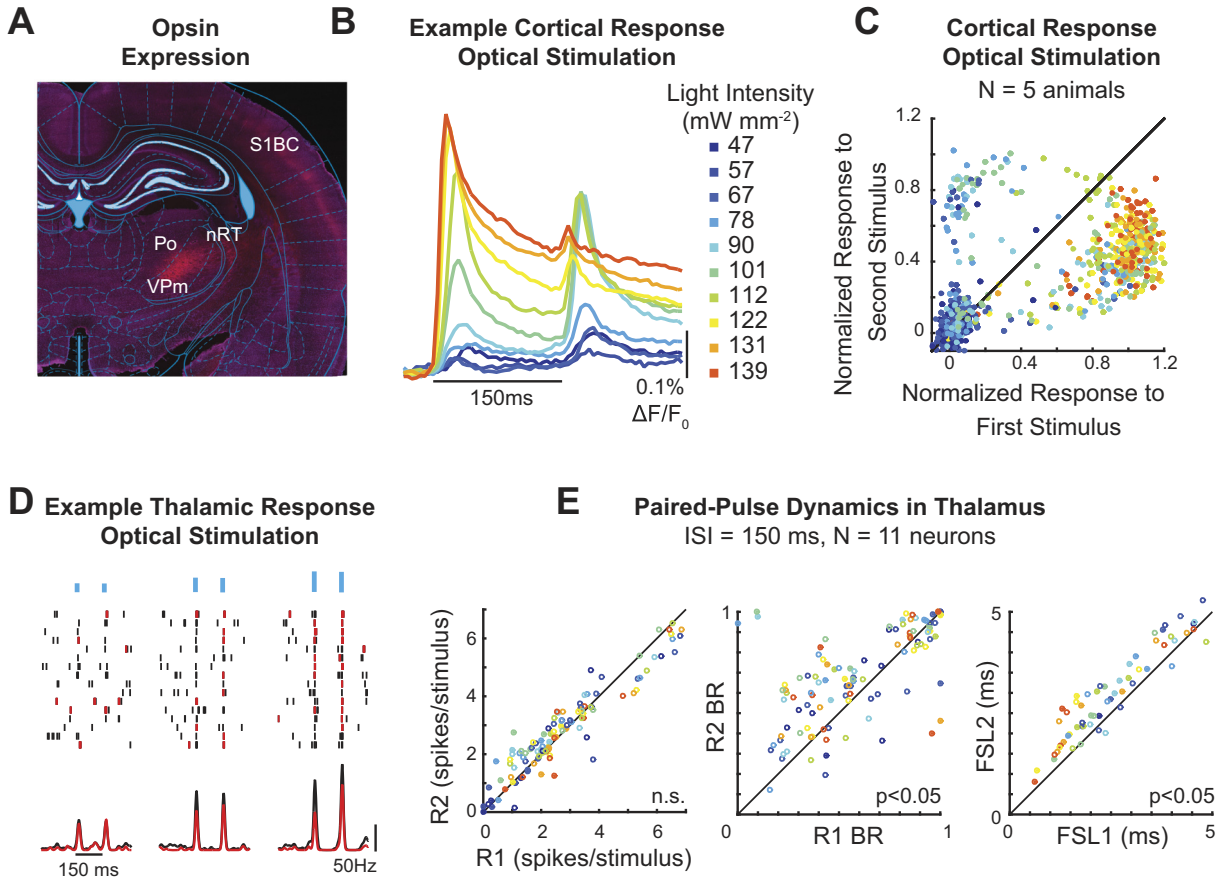

Fig. 5. Optogenetic stimulation of the thalamus also exhibits bimodal nonlinear dynamics. *A*: example histological image of opsin spread within thalamus. VPm, ventral posteromedial thalamus; Po, posterior thalamus, nRT, reticular nucleus of the thalamus; S1BC, barrel cortex. *B*: example of the cortical response, averaged within a single cortical column, to increasing stimulus intensities (ISI = 150 ms). *C*: the response to the second stimulus is plotted against the response to the first stimulus for single trials of varying light intensity. Points above the unity line (diagonal) were facilitated, while points below the unity line were suppressed (n = 5 animals). The responses were normalized, for each animal, relative to the mean response for the strongest light intensity during that experiment. Optogenetic stimulation exhibited a mixture of facilitation and suppression, with the facilitation less reliable on a trial-to-trial basis. *D*: rastergram and peristimulus time histogram for an example single-unit VPm cell in response to paired optogenetic stimuli of increasing intensity. Within the rastergram, red spikes belong to an identified burst. *E*: across neurons (N = 11 neurons), the overall evoked response, defined as the average number of spikes elicited within 20 ms of stimulus onset, was not different for the first and second stimuli (*left*; n.s., P = 0.47, 3-way ANOVA; factors: animal, stimulus condition, stimulus number), but the burst activity was higher in response to the second stimulus (*center*; P = 2.79e-4, 3-way ANOVA; factors: animal, stimulus condition, stimulus number). The first spike latency (FSL) was also higher in response to the second pulse compared with the first (*right*; P = 0.001, 3-way ANOVA; factors: animal, stimulus condition, stimulus number). Note that 8 of 11 neurons were collected with a different anesthesia. These data points are indicated by open circles, while neurons collected with the same anesthesia as the imaging experiments are indicated by filled circles.

stimulation of the thalamus as opposed to electrical stimulation and found a bimodality in the nonlinear dynamics similar to that seen for thalamic microstimulation (Fig. 5*A*; example of opsin expression within thalamus). As shown for one example, the cortical response to increasing light intensities demonstrated both facilitation and suppression dynamics (Fig. 5*B*). In Fig. 5*C*, the response to the second stimulus is plotted relative to the response to the first stimulus for each trial across stimulus intensities. Similar to the thalamic microstimulation results described in Fig. 3, three clusters are apparent in this representation of the data. At very low stimulus intensities, there was no response to either of the two stimuli. At intermediate stimulus intensities, the majority of trials exhibited facilitation, forming a cluster in the top left quadrant of the axes. At the highest stimulus intensities, the cortical response to the second stimulus was suppressed relative to the response to the first, forming a cluster in the bottom right quadrant of the axes (Fig. 5*C*; n = 5 animals).

Importantly, optogenetic stimulation of thalamus can be used in conjunction with electrophysiological recordings in thalamus because it does not introduce the same electrical artifact caused by thalamic microstimulation. In our paired-pulse paradigm, the direct optical activation of thalamic neurons is transmitted downstream to produce the cortical dynamics measured with optical techniques. Therefore, we have direct access to the input to the cortical circuit with the ability to record from the thalamic neurons that are being stimulated and can begin to investigate the source of the facilitation/suppression dynamics measured in cortex. It is possible that similar facilitation/suppression dynamics are present in the spiking activity of thalamic neurons and that these thalamic dynamics are simply inherited at the level of cortex as the information is transmitted downstream. However, it is also possible that the dynamics of the thalamic spiking activity are dissimilar to those seen in cortex such that the cortical dynamics are instead generated by integrating across thalamic inputs.

Using extracellular recordings in thalamus, we quantified the dynamics of the thalamic spiking response to attempt to identify the source of the facilitation/suppression dynamics seen cortically.

For an example neuron, the evoked spiking activity in response to the light increases with increasing light intensity (Fig. 5*D*). This example neuron was driven by the same paired optogenetic stimuli used in Fig. 5*B*, consisting of two 5-ms pulses of light at varying light intensity, separated by a 150-ms ISI. Putative T-type calcium channel bursts, shown in red (Fig. 5*D*), were classified as any set of spikes where the first spike is preceded by 100 ms of silence or more and every subsequent spike in the burst is separated by an ISI that is <4 ms (Lu et al. 1992; Reinagel et al. 1999). In response to a weak light input, the cell responded occasionally to the stimulation. In response to the intermediate light intensity (Fig. 5*D*, *center*), the cell responded reliably across trials, but with an approximately equal number of burst spikes in response to either pulse (red spikes in the raster plot belong to a burst). In response to a higher light intensity, the bursting response to the second stimulus was facilitated relative to the first stimulus. Across neurons, the number of thalamic spikes evoked in response to the second stimulus was plotted against the number of thalamic spikes elicited in response to the first stimulus for varying light intensity (Fig. 5*E*, *left*; $N = 11$ neurons). In contrast to the cortical results, no strong suppression or facilitation of the evoked thalamic spike count in response to the optical stimulus occurred, as all data points were approximately on the unity line (Fig. 5*E*, *left*, diagonal line; $N = 11$ neurons, $P = 0.47$, 3-way ANOVA). However, when plotting the burst ratio, defined as the number of burst spikes divided by the total number of spikes, of the evoked response to the first pulse vs. the evoked response to the second pulse, there is a facilitation of the bursting dynamic (Fig. 5*E*, *center*; $N = 11$ neurons, $P = 2.79\text{e-}4$, 3-way ANOVA). Furthermore, the first spike latency in response to the second stimulus was longer than for the first stimulus, consistent with the slow calcium dynamics underlying a burst response that increases latency (Fig. 5*E*, *right*; $N = 11$ neurons, $P = 0.001$, 3-way ANOVA). Given that the absolute number of spikes did not exhibit strong interactions between the first and second stimuli but the bursting activity was reliably enhanced in response to the second stimulus, we suggest that thalamic bursting dynamics induced by the paired-pulse paradigm could underlie the facilitation dynamics in cortex. Specifically, we hypothesize that the interactions between VPm and nRT will enhance bursting at ISIs on the order of 100–150 ms (see DISCUSSION). Note that there was no strong suppression dynamic in the thalamic neurons. We propose that, at least in part, the cortical suppression dynamic is due to rapid synaptic depression (see DISCUSSION).

Modulation of thalamic state eliminates facilitation dynamics. To directly test the role of thalamic bursting on cortical facilitation dynamics, we transitioned from using optogenetics to drive the thalamic neurons (Fig. 5) to using optogenetics in a more subtle way to modulate the state of the thalamus (Fig. 6). Thalamic state is believed to play a critical role in the nonlinear dynamics of the cortical response (Sherman 2001). Previous work in the rodent vibrissa system has shown that optogenetic depolarization of the thalamus is sufficient to shift thalamic firing modes from burst to tonic (Whitmire et al. 2016) as well as cortical state from synchronized to desynchronized (Poulet et al. 2012). Here we experimentally depolarized the state of the thalamus optogenetically to shift the firing mode while quantifying the role of thalamic state in the generation of the cortical facilitation dynamic in response to thalamic microstimulation.

Under anesthesia, the VPM neurons were principally in the burst firing mode, where the neuron fires classically defined bursts of spikes in response to a stimulus (Fig. 6*A*, *left*). With the same experimental setup as before, an optical fiber attached to an electrode was used to deliver a constant amount of light to chronically depolarize the thalamic neurons and move them into the tonic firing mode (Fig. 6*B*, *left*). The optically depolarized state led to increased firing rates and decreased bursting relative to the baseline condition, as described previously (Whitmire et al. 2016). To illustrate the difference in firing statistics between these two modes, we analyzed the ISI distributions. For each spike, the time since the previous spike (previous ISI) and the time until the next spike (next ISI) are plotted against each other in Fig. 6, *A* and *B*, *right*, to investigate temporal patterns in the spiking data. Within these axes, the red boxes indicate a classically defined T-type calcium channel burst, where the box in the bottom right corner signifies the start of a burst with a long (>100 ms) previous ISI followed by a short (<4 ms) ISI and the box in the bottom left corner contains any subsequent spikes in the burst. The final spike in the burst will lie along the left axis. In the burst firing mode, a large portion of the spikes (52% in this example) are classified as part of a burst (Fig. 6*A*, *right*). The tonic firing mode, however, has a much smaller proportion of spikes classified as burst spikes, and instead the majority of the spikes lie in a cloud along the diagonal of the axes (Fig. 6*B*, *right*; 3% in this example).

Using depolarizing opsins, we controlled the relative depolarization of the thalamus to directly investigate the effect of thalamic state on neural activity propagation in the thalamocortical circuit. VSDI was used to record the cortical response to thalamic microstimulation in the baseline anesthetized state (Baseline) and the optogenetically depolarized state (Depolarized). Consistent with our data described above (Fig. 3*C*), the cortical response to thalamic microstimulation in the Baseline state exhibited bimodal nonlinear dynamics where intermediate current amplitudes elicited facilitation dynamics while strong current amplitudes elicited profound suppression (Fig. 6*C*).

If the cortical facilitation dynamic were caused by thalamic bursting, then the optogenetic depolarization of the thalamus, which prevents burst firing by inactivating the T-type calcium channels and preventing activation of the h current at hyperpolarized potentials, would also prevent the cortical facilitation. Indeed, this was the case. Figure 6*D* presents the matched experiment to Fig. 6*C* but under optogenetic depolarization (Depolarized state). In this case, regardless of the stimulus intensity or response amplitude, the response to the second stimulus was suppressed relative to the response to the first. This occurred reliably across trials and experiments, as the overwhelming majority of data points fell below the unity line (Fig. 6*D*, *center* and *right*). Importantly, the response to the first stimulus was similar in both the control and the depolarization conditions ($P > 0.05$, Wilcoxon rank sum test) and therefore only the response to the second stimulus was affected. With manipulation of the state of the thalamus, and

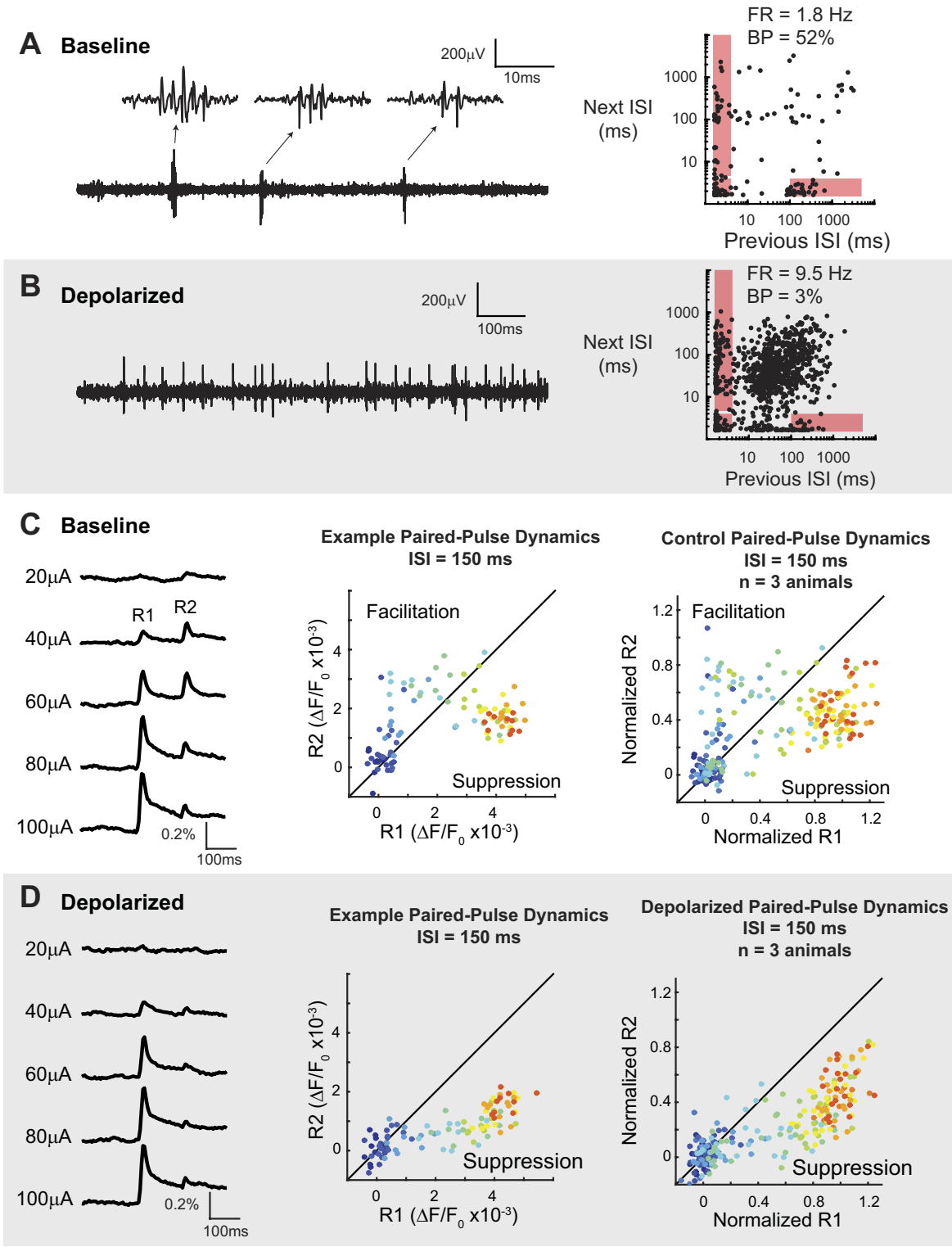

Fig. 6. Depolarization of the thalamus eliminates thalamic bursting and cortical paired-pulse facilitation. *A*: under anesthesia, thalamic neurons spontaneously burst, firing multiple action potentials in quick succession (*left*). *Right*: for each spike, the interspike interval (ISI) to the previous spike is plotted against the ISI to the next spike. The red boxes outline spikes that could make up a burst. In the anesthetized state, the proportion of spikes that make up bursts (BP) is 52%. FR, firing rate. *B*: when depolarized through optogenetic manipulation the thalamic neurons switch to a tonic firing mode (*left*), and the majority of spikes occur in tonic firing and very few (3%) during bursts (*right*). *C*: example of the mean cortical response, as measured through VSDI, to pairs of thalamic microstimuli with increasing strength (interstimulus interval is 150 ms). As described above, facilitation occurs at subthreshold currents whereas suppression characterizes suprathreshold currents in the control state (*center*), and this is consistent across animals (*right*; $n = 3$ animals). *D*: when the thalamus is depolarized, there is no longer facilitation in the evoked cortical response (*left*). In an example recording with thalamic depolarization, the cortical response undergoes paired-pulse suppression for all current intensities (*center*), and this is consistent across animals (*right*; $n = 3$ animals). Data are normalized with respect to the maximum response amplitude within that experiment.

therefore the associated bursting activity, the nonlinear propagation of neural activity within the thalamocortical circuit shifted from a facilitative dynamic in the anesthetized control condition to a suppressive dynamic in the depolarized tonic thalamic state condition.

DISCUSSION

Across nearly all sensory modalities, the thalamus is a common stage of processing that links the peripheral sensory world to the cortex. Before reaching the thalamus, sensory information is transduced at the receptor and processed by a diverse set of prethalamic circuits. For example, in the visual system a significant amount of processing occurs at the periphery, where photons are transduced into electrical signals (Schnapf et al. 1990) before a network of excitatory and inhibitory interactions in the retina shape information flow to the visual thalamus (Laughlin 1987). In the somatosensory pathway, the prethalamic processing is arguably less complex, where mechanical deformations at the whisker follicle are transduced by sensory neurons (Lottem and Azouz 2011) that synapse directly in the brain stem before the sensory information is transmitted to the thalamus (Diamond et al. 2008). The first-order neurons in the vibrissa pathway encode an incredibly precise representation of the relevant features of the whisker movement (Bale et al. 2015; Jones et al. 2004) that is transformed by the highly ordered brain stem circuitry (Sakurai et al. 2013). Although not historically viewed as such, the transformation from the brain stem to thalamus actually represents a significant stage of sensory processing (Sosnik et al. 2001). Therefore, observations of thalamic and cortical activity are always confounded by prethalamic dynamics, making it difficult to establish what happens where. Here we used a range of experimental tools and compared response properties across different conditions in the intact circuit in vivo, to ultimately disentangle the simplest aspects of these observed dynamics.

Role of thalamic firing modes in thalamocortical information transmission. It has long been hypothesized that the distinct firing modes of thalamus, known as burst and tonic firing modes, present a mechanism to differentially transmit information to cortex. While the transition between firing modes, or thalamic states, can be achieved through a variety of natural and artificial mechanisms, the impact on information transmission remains speculative. Before the development of optogenetic tools, the primary method to control thalamocortical state was through the activation of the natural neuromodulatory arousal mechanisms in the brain (Castro-Alamancos 2002; Goard and Dan 2009; Llinas and Steriade 2006). However, with the advent of optogenetics, it has become possible to quickly and easily shift the thalamocortical state locally and bidirectionally. Activating the reticular thalamus, or hyperpolarizing the thalamocortical projection nuclei of the thalamus, increases both bursting activity in the thalamus and spindle generation in the local field potential in cortex (Halassa et al. 2011). On the other hand, direct depolarization of the thalamus causes the transition from burst to tonic firing rate (Whitmire et al. 2016), producing the classically described desynchronized state (Poulet et al. 2012). Yet in neither case has the effect on the propagation of stimulus-evoked activity been quantified. Here we directly tested the role of thalamic state in the propagation of neural activity in response to thalamic microstimulation during the tonic and burst firing modes of the thalamus.

In the burst firing mode (i.e., the baseline anesthetized state), thalamic microstimulation activated bimodal nonlinear cortical dynamics with facilitation of subthreshold inputs and suppression of suprathreshold inputs in the cortical response. Artificial stimulation of the thalamus causes extreme precision of the thalamic spiking output relative to whisker-driven activity (Millard et al. 2015). When considered across a population of thalamic neurons, the extreme synchrony induced by artificial stimuli enhances the strength of both the feedforward input to cortex and the input to the feedback pathway with the nRT, which is the only known source of inhibition to the VPm (Pinault 2004). We propose that this strong synchronous activation of the nRT will elicit a robust inhibitory feedback response to the VPm neurons. In the context of the paired-pulse stimulus, this nRT-mediated inhibition will strongly hyperpolarize the VPm neurons shortly after the first stimulus, which will prime the T-type calcium channels to open. The hyperpolarizing input from nRT will also activate h currents, which will depolarize the neurons and prepare the thalamus to burst (Lüthi and McCormick 1998). When the second stimulus arrives 100–150 ms later, after the inhibition has decayed, the current pulse will provide the necessary depolarizing input to elicit a strong bursting response in the thalamic projection neurons. The facilitation of bursting in response to the second stimulus could therefore underlie the facilitation dynamic seen in cortex. Recent biophysical modeling of the thalamocortical circuit also suggests that feedback from nRT could provide a mechanism for facilitated thalamocortical activation due to low-threshold bursting for stimuli arriving at ~10 Hz (Willis et al. 2015). We directly tested the role of bursting in the facilitation dynamic by optogenetically depolarizing the thalamus to reduce thalamic bursting, as we have done previously (Whitmire et al. 2016). As predicted, the cortical facilitation dynamics were eliminated in the depolarized thalamus condition. By directly depolarizing the VPm neurons, we propose that we were able to counteract the stimulus-evoked inhibition from nRT, preventing both the activation of h current and the opening of the T-type calcium channels in response to the second stimulus. This is consistent with previous work showing a reduction in the paired-pulse facilitation of the cortical response to thalamic microstimulation during natural transitions of an awake animal between quiescent and active states (Castro-Alamancos and Connors 1996b), which would presumably lead to a shift in thalamic state.

Importantly, a shift in thalamic state leads to a shift in the overall amount of thalamic spiking activity. In the tonic mode, the increased firing activity will likely cause any thalamocortical synapses to be in a more depressed state and therefore could play a role in the elimination of the facilitation dynamic in the transition from burst to tonic firing. While we could not control for the overall firing rates in the two thalamic firing modes, we did perform an experiment to test the role of the synapse state in the generation of the facilitation dynamic (Fig. 3*D*). In this paradigm, the cortical response to thalamic microstimulation was compared between current pulses presented in isolation and those preceded by a facilitating current pulse amplitude (60 μA). When the pulse is presented in isolation, the thalamus should be in the baseline anesthetized condition (burst firing mode) such that the thalamocortical synapses are

not predepressed. The cortical response to the facilitating current pulse is minimal but still could potentially impact the thalamocortical synapses, leading to a synaptically depressed state. However, when the pulse was presented 150 ms after the facilitating current pulse, the evoked cortical response was facilitated across current amplitudes. Given that the thalamocortical synapses were either in similar or slightly depressed states relative to the stimulus isolation condition, this result suggests that the facilitation dynamic cannot be attributed to short-term depression dynamics. Furthermore, when optogenetics were used to modulate the state of the thalamus, the light stimulus began at least 200 ms before the onset of the first electrical stimulus in the paired-stimulus train. As such, the thalamic neurons should have been optically depolarized, and the synapses sufficiently depressed, at the time of the first stimulus presentation. However, a comparison of the evoked cortical response to the first electrical stimulus in the Baseline and Depolarized conditions found no difference. This suggests that it is the dynamics of this temporal pattern of stimuli that elicits the facilitation dynamic. While the state of the synapse at the time of stimulus arrival will certainly play a critical role in whether or how that information is transmitted, and likely underlies the paired-pulse suppression dynamics presented here, it cannot explain the facilitation dynamic.

Alternative mechanisms that could underlie cortical facilitation dynamic elicited by artificial thalamic stimulation. While we explicitly tested modulations to thalamic bursting as a mechanism to explain the facilitation dynamics described here, there are at least three alternative candidate mechanisms through which the artificial stimuli could have recruited the additional nonlinear dynamics: *1*) simultaneous activation of axons from the POm in the thalamus, which has been associated with the thalamocortical augmenting response (Castro-Alamancos and Connors 1996b), *2*) nonspecific circuit excitation through artificial stimulation, or *3*) preferential activation of class II facilitating synapses that extend directly from VPm to layer 2/3 cells (Viaene et al. 2011).

The thalamocortical augmenting response was originally described more than 70 years ago (Dempsey and Morison 1943) but has more recently been studied in the rodent whisker system (Castro-Alamancos and Connors 1996b). The augmenting response is characterized by progressive facilitation of the cortical response to thalamic microstimulation for ISIs between 50 and 200 ms and has been shown to occur in the awake animal (Castro-Alamancos and Connors 1996b). The exact mechanism of the augmenting response is disputed, however, with some pointing to cortical mechanism while others propose that the dynamics are thalamic in origin. Principally, though, the augmenting response is believed to be a product of bursting thalamocortical recipient cells within layer 5 of cortex. In the rodent vibrissa system, this has primarily been considered through stimulation of the POm nucleus, which projects to layer 5 of cortex as a part of the paralemniscal pathway, whereas VPm primarily projects to layer 4 [although recent evidence has also demonstrated direct projections from VPm to layer 5 (Constantinople and Bruno 2013)]. Because of the close proximity of POm and VPm, it is possible that thalamic microstimulation recruited the augmenting response by activating POm axons passing through/near VPm. However, given the observation of facilitated bursting in the VPm units, facilitation caused by optogenetic stimuli (which are believed to stimulate axons to a lesser extent), and the elimination of facilitation induced by electrical stimulation with modulation of thalamic state (which would not directly impact the region of tissue activated by electrical stimulation), the classical augmenting response likely was not the primary mechanism of the facilitation.

Although commonly used, electrical stimulation is nonspecific in its excitation such that antidromic activation is possible. In the context of the facilitation dynamic explored here, antidromic stimulation of cholinergic axons projecting to thalamus could play an important role by subsequently providing cholinergic activation to cortex. Cholinergic activation has been shown to increase firing rates in the VPm of the thalamus, which shifts the cortex into a desynchronized state (Hirata and Castro-Alamancos 2010). At the level of cortex, continuous optogenetic activation of the basal forebrain led to an increase in both the spontaneous and stimulus-evoked firing rate (Pinto et al. 2013). Furthermore, in conjunction with sensory stimulation, cholinergic activation of cortex has been shown to facilitate the responsiveness to sensory inputs (Metherate and Ashe 1993). However, in contrast to the prolonged cholinergic activation used in these prior studies, our electrical stimulation of thalamus provided brief (400 μs) stimuli that would limit the temporal duration of any potential effects of cholinergic axon activation. Furthermore, as described above, with optogenetics the activation is restricted to neurons expressing the opsin (and therefore will not activate the nearby terminals). Therefore the similarity in the evoked response for both electrical and optical stimulation suggests that antidromic activation of brain regions projecting to thalamus by electrical stimulation, such as cholinergic neurons in the basal forebrain and brain stem, likely do not play a significant role in the dynamics described here.

Direct synaptic connections from VPm to layer 2/3 have recently been reported with facilitation properties such that 10-Hz stimuli delivered to VPm in vitro elicited facilitation of the postsynaptic potential in the layer 2/3 neurons (Viaene et al. 2011). This was in contrast to the synaptic response in layer 4 neurons, which demonstrated suppression. While this may have played a role in the cortical facilitation dynamic, the elimination of facilitation with increased thalamic firing rates in VPm during optogenetic depolarization suggests that facilitating synapses in L2/3 alone are insufficient to explain the observed trends. As such, we propose that thalamic bursting coupled between the VPm and nRT thalamic nuclei is the fundamental mechanism underlying the paired-pulse facilitation dynamic seen for artificial stimuli.

Differential circuit activation by sensory and artificial stimulation. The profound facilitation dynamics in cortex in response to this paired-pulse paradigm were primarily recruited by direct stimulation of the thalamic neurons. In building a comparison between the sensory stimulation and the artificial stimulation, we have recently published a fairly extensive analysis of the evoked cortical response (Millard et al. 2015). We found that both sensory and artificial stimuli can elicit a full range of cortical response amplitudes but that they differ in the variability of the evoked cortical response. To identify a potential cause for this difference in variability trend, we directly compared the thalamic re-

sponse to a single optical stimulus and a single whisker stimulus. We found that the optogenetic activation of the thalamic neurons led to a highly precise spiking response, which we modeled as a potential factor underlying the variability trends seen cortically. In this work, we hypothesized that synchronous activation of the thalamic neurons by the optogenetic activation (and likely the electrical stimulation) provided a strong input to the reticular thalamus (nRT), which facilitated bursting in response to the second stimulus, whereas the effects of whisker stimulation were confounded by prethalamic processing. Prethalamic processing represents an important stage of encoding in the whisker pathway that is not activated by direct thalamic stimulation. While some individual trials showed facilitation, whisker stimulation primarily led to suppression dynamics in the cortical response. However, the dynamics of the whisker to barreloid response are difficult to separate from the thalamocortical dynamics we sought to quantify here, leading to uncertainty about the source of the suppression dynamic seen for sensory stimulation. A particularly relevant candidate mechanism is depression at the trigeminothalamic synapse (Deschênes et al. 2003) such that the synaptic drive in thalamus in response to the second sensory stimulus would be lower than the synaptic drive in response to the first sensory stimulus, leading to suppression dynamics before the signal even reaches thalamus. Importantly, synaptic depression is particularly salient in the anesthetized animal, where spontaneous firing rates are considerably lower than in the awake animal (Borst 2010; Reinhold et al. 2015). We propose that the response to each whisker stimulus in the paired-pulse train likely elicits different responses at the level of the thalamus due, at least in part, to the synaptic depression dynamics that cannot be decoupled from the thalamocortical processing. Direct stimulation of the thalamic neurons using artificial stimulation techniques allowed us to override any potentially suppressive dynamics that occur in prethalamic processing to focus on the dynamics established in the thalamocortical processing. In this restricted paradigm, we were able to recruit profound facilitation dynamics. However, the 150-ms ISI that demonstrated cortical facilitation in response to artificial thalamic activation here has also been identified as relevant from extracellular recordings from cortical layer 4 in response to time-varying pairs of whisker stimuli (Boloori et al. 2010; Boloori and Stanley 2006; Webber and Stanley 2004). Rather than simply showing a monotonic recovery from suppression in the cortical spiking activity with increasing duration between the first and the second whisker stimulus, the equivalent measures of PPR in these studies had a local maximum at stimulus intervals of 100–150 ms for different whisker deflection directions (Webber and Stanley 2004) and different stimulus velocities (Boloori et al. 2010). These results suggest that the temporal spacing of stimulus patterns is critical in shaping the neural dynamics of the sensory pathway and that this 100- to 150-ms ISI is critical for sensory information transmission. When the sensory stimulus pattern is expanded to include a third whisker stimulus, the cortical response can demonstrate facilitated spiking as the dynamics interact to drive a "suppression of suppression" (Boloori and Stanley 2006; Webber and Stanley 2006). When extended to even more complex patterns of stimulation, this can create fairly complex, yet reliable response patterns. While the prethalamic processing may restrict the intensity of the facilitation dynamic seen cortically in response to two whisker stimuli, these complex interactions across more naturalistic stimuli could provide a mechanism to facilitate information that arrives to thalamus at a frequency of ~10 Hz. In the vibrissa pathway, this stimulus frequency becomes very relevant where active sensing is achieved through sweeping whisking motions at 5–15 Hz (Berg and Kleinfeld 2003).

In probing neural circuits, simple paired-pulse paradigms have built the foundation for our understanding of more complex sensory-evoked cortical dynamics (Simons 1985). Here, using a combination of optogenetic thalamic state modulation and electrical paired-pulse stimulation of thalamus, we have identified the bursting dynamics of the thalamic circuitry as a potential mechanism to facilitate information transfer to cortex. While these thalamic state transitions are not entirely understood, it is evident that thalamic state transitions can occur rapidly as a function of both sensory input and neuromodulatory influences. Combined with the continuous nature of arriving sensory inputs, the rapid state transitions may selectively facilitate the transmission of information related to particular patterns of sensory inputs over this timescale. The simple dynamic interaction identified here must be expanded to incorporate the temporal interactions across stimuli that capture the interplay between excitatory and inhibitory circuitry as the patterns of stimuli become increasingly complex (Boloori et al. 2010). When combined with the state dependence of the neural dynamics, temporal patterns of stimulation are capable of eliciting diverse cortical responses, which are ultimately the likely substrate upon which sensory percepts are built.

ACKNOWLEDGMENTS

Statistical support was provided by the National Center for Advancing Translational Sciences of the National Institutes of Health (NIH) under Award Number UL1 TR-000454. Imaging support for the histology shown was provided by the Parker H. Petit Institute for Bioengineering and Biosciences Microscopy Core at the Georgia Institute of Technology.

GRANTS

This work was supported by National Institute of Neurological Disorders and Stroke Grants R01 NS-48285 and R01 NS-085447. C. J. Whitmire was supported by GT/Emory NIH Computational Neuroscience Training Grant T90 DA-032466 and NIH NRSA Predoctoral Fellowship F31 NS-089412. D. C. Millard was supported by a National Science Foundation Graduate Research Fellowship.

DISCLOSURES

No conflicts of interest, financial or otherwise, are declared by the author(s).

AUTHOR CONTRIBUTIONS

C.J.W., D.C.M., and G.B.S. conceived and designed research; C.J.W. and D.C.M. performed experiments; C.J.W. and D.C.M. analyzed data; C.J.W., D.C.M., and G.B.S. interpreted results of experiments; C.J.W. and D.C.M. prepared figures; C.J.W., D.C.M., and G.B.S. drafted manuscript; C.J.W., D.C.M., and G.B.S. edited and revised manuscript; C.J.W., D.C.M., and G.B.S. approved final version of manuscript.

REFERENCES

Aravanis AM, Wang LP, Zhang F, Meltzer LA, Mogri MZ, Schneider MB, Deisseroth K. An optical neural interface: in vivo control of rodent

motor cortex with integrated fiberoptic and optogenetic technology. *J Neural Eng* 4: S143–S156, 2007.

Bale MR, Campagner D, Erskine A, Petersen RS. Microsecond-scale timing precision in rodent trigeminal primary afferents. *J Neurosci* 35: 5935–5940, 2015.

Berg RW, Kleinfeld D. Rhythmic whisking by rat: retraction as well as protraction of the vibrissae is under active muscular control. *J Neurophysiol* 89: 104–117, 2003.

Boloori AR, Jenks RA, Desbordes G, Stanley GB. Encoding and decoding cortical representations of tactile features in the vibrissa system. *J Neurosci* 30: 9990–10005, 2010.

Boloori AR, Stanley GB. The dynamics of spatiotemporal response integration in the somatosensory cortex of the vibrissa system. *J Neurosci* 26: 3767–3782, 2006.

Borst JG. The low synaptic release probability in vivo. *Trends Neurosci* 33: 259–266, 2010.

Castro-Alamancos MA. Different temporal processing of sensory inputs in the rat thalamus during quiescent and information processing states in vivo. *J Physiol* 539: 567–578, 2002.

Castro-Alamancos MA, Connors BW. Cellular mechanisms of the augmenting response: short-term plasticity in a thalamocortical pathway. *J Neurosci* 16: 7742–7756, 1996a.

Castro-Alamancos MA, Connors BW. Spatiotemporal properties of short-term plasticity sensorimotor thalamocortical pathways of the rat. *J Neurosci* 16: 2767–2779, 1996b.

Chung S, Li X, Nelson SB. Short-term depression at thalamocortical synapses contributes to rapid adaptation of cortical sensory responses in vivo. *Neuron* 34: 437–446, 2002.

Civillico EF, Contreras D. Comparison of responses to electrical stimulation and whisker deflection using two different voltage-sensitive dyes in mouse barrel cortex in vivo. *J Membr Biol* 208: 171–182, 2005.

Constantinople CM, Bruno RM. Deep cortical layers are activated directly by thalamus. *Science* 340: 1591–1594, 2013.

Crick F. Function of the thalamic reticular complex: the searchlight hypothesis. *Proc Natl Acad Sci USA* 81: 4586–4590, 1984.

Crochet S, Petersen CC. Correlating whisker behavior with membrane potential in barrel cortex of awake mice. *Nat Neurosci* 9: 608–610, 2006.

Dempsey EW, Morison RS. The electrical activity of a thalamocortical relay system. *Am J Physiol* 138: 283–296, 1943.

Deschênes M, Timofeeva E, Lavallée P. The relay of high-frequency sensory signals in the whisker-to-barreloid pathway. *J Neurosci* 23: 6778–6787, 2003.

Diamond ME, von Heimendahl M, Knutsen PM, Kleinfeld D, Ahissar E. "Where" and "what" in the whisker sensorimotor system. *Nat Rev Neurosci* 9: 601–612, 2008.

Ego-Stengel V, Mello e Souza T, Jacob V, Shulz DE. Spatiotemporal characteristics of neuronal sensory integration in the barrel cortex of the rat. *J Neurophysiol* 93: 1450–1467, 2005.

Fanselow EE, Sameshima K, Baccala LA, Nicolelis MA. Thalamic bursting in rats during different awake behavioral states. *Proc Natl Acad Sci USA* 98: 15330–15335, 2001.

Ganmor E, Katz Y, Lampl I. Intensity-dependent adaptation of cortical and thalamic neurons is controlled by brainstem circuits of the sensory pathway. *Neuron* 66: 273–286, 2010.

Goard M, Dan Y. Basal forebrain activation enhances cortical coding of natural scenes. *Nat Neurosci* 12: 1444–1449, 2009.

Gollnick CA, Millard DC, Ortiz AD, Bellamkonda RV, Stanley GB. Response reliability observed with voltage-sensitive dye imaging of cortical layer 2/3: the probability of activation hypothesis. *J Neurophysiol* 115: 2456–2469, 2016.

Halassa MM, Siegle JH, Ritt JT, Ting JT, Feng G, Moore CI. Selective optical drive of thalamic reticular nucleus generates thalamic bursts and cortical spindles. *Nat Neurosci* 14: 1118–1120, 2011.

Hawken MJ, Shapley RM, Grosof DH. Temporal-frequency selectivity in monkey visual cortex. *Vis Neurosci* 13: 477–492, 1990.

Higley MJ, Contreras D. Frequency adaptation modulates spatial integration of sensory responses in the rat whisker system. *J Neurophysiol* 97: 3819–3824, 2007.

Hirata A, Castro-Alamancos MA. Neocortex network activation and deactivation states controlled by the thalamus. *J Neurophysiol* 103: 1147–1157, 2010.

Jones LM, Depireux DA, Simons DJ, Keller A. Robust temporal coding in the trigeminal system. *Science* 304: 1986–1989, 2004.

Jouhanneau JS, Kremkow J, Dorrn AL, Poulet JF. In vivo monosynaptic excitatory transmission between layer 2 cortical pyramidal neurons. *Cell Rep* 13: 2098–2106, 2015.

Kilgard MP, Merzenich MM. Plasticity of temporal information processing in the primary auditory cortex. *Nat Neurosci* 1: 727–731, 1998.

Laughlin SB. Form and function in retinal processing. *Trends Neurosci* 10: 478–483, 1987.

Lesica NA, Weng C, Jin J, Yeh CI, Alonso JM, Stanley GB. Dynamic encoding of natural luminance sequences by LGN bursts. *PLoS Biol* 4: e209, 2006.

Lippert MT, Takagaki K, Xu W, Huang X, Wu JY. Methods for voltage-sensitive dye imaging of rat cortical activity with high signal-to-noise ratio. *J Neurophysiol* 98: 502–512, 2007.

Llinas R, Steriade M. Bursting of thalamic neurons and states of vigilance. *J Neurophysiol* 95: 3297–3308, 2006.

Lottem E, Azouz R. A unifying framework underlying mechanotransduction in the somatosensory system. *J Neurosci* 31: 8520–8532, 2011.

Lu S, Guido W, Sherman SM. Effects of membrane voltage on receptive field properties of lateral geniculate neurons in the cat: contributions of the low-threshold Ca^{2+} conductance. *J Neurophysiol* 68: 2185–2198, 1992.

Lüthi A, McCormick DA. H-current: properties of a neuronal and network pacemaker. *Neuron* 21: 9–12, 1998.

Mattis J, Tye KM, Ferenczi EA, Ramakrishnan C, O'Shea DJ, Prakash R, Gunaydin LA, Hyun M, Fenno LE, Gradinaru V, Yizhar O, Deisseroth K. Principles for applying optogenetic tools derived from direct comparative analysis of microbial opsins. *Nat Methods* 9: 159–172, 2012.

McAlonan K, Cavanaugh J, Wurtz RH. Guarding the gateway to cortex with attention in visual thalamus. *Nature* 456: 391–394, 2008.

Metherate R, Ashe JH. Nucleus basalis stimulation facilitates thalamocortical synaptic transmission in the rat auditory cortex. *Synapse* 14: 132–143, 1993.

Millard DC, Wang Q, Gollnick CA, Stanley GB. System identification of the nonlinear dynamics in the thalamocortical circuit in response to patterned thalamic microstimulation in vivo. *J Neural Eng* 10: 66011, 2013.

Millard DC, Whitmire CJ, Gollnick CA, Rozell CJ, Stanley GB. Electrical and optical activation of mesoscale neural circuits with implications for coding. *J Neurosci* 35: 15702–15715, 2015.

Newman JP, Fong M, Millard DC, Whitmire CJ, Stanley GB, Potter SM. Optogenetic feedback control of neural activity. *Elife* 4: e07192, 2015.

Paxinos G, Watson C. *The Rat Brain in Stereotaxic Coordinates*. San Diego: Academic, 1998.

Petersen CC, Grinvald A, Sakmann B. Spatiotemporal dynamics of sensory responses in layer 2/3 of rat barrel cortex measured in vivo by voltage-sensitive dye imaging combined with whole-cell voltage recordings and neuron reconstructions. *J Neurosci* 23: -1298–309, 2003.

Pinault D. The thalamic reticular nucleus: structure, function and concept. *Brain Res Brain Res Rev* 46: 1–31, 2004.

Pinto L, Goard MJ, Estandian D, Xu M, Kwan AC, Lee SH, Harrison TC, Feng G, Dan Y. Fast modulation of visual perception by basal forebrain cholinergic neurons. *Nat Neurosci* 16: 1857–1863, 2013.

Poulet JF, Fernandez LM, Crochet S, Petersen CC. Thalamic control of cortical states. *Nat Neurosci* 15: 370–372, 2012.

Poulet JF, Petersen CC. Internal brain state regulates membrane potential synchrony in barrel cortex of behaving mice. *Nature* 454: 881–885, 2008.

Quiroga RQ, Nadasdy Z, Ben-Shaul Y. Unsupervised spike detection and sorting with wavelets and superparamagnetic clustering. *Neural Comput* 16: 1661–1687, 2004.

Ramcharan EJ, Gnadt JW, Sherman SM. Burst and tonic firing in thalamic cells of unanesthetized, behaving monkeys. *Vis Neurosci* 17: 55–62, 2000.

Reinagel P, Godwin D, Sherman SM, Koch C. Encoding of visual information by LGN bursts. *J Neurophysiol* 81: 2558–2569, 1999.

Reinhold K, Lien AD, Scanziani M. Distinct recurrent versus afferent dynamics in cortical visual processing. *Nat Neurosci* 18, 2015.

Sakurai K, Akiyama M, Cai B, Scott A, Han BX, Takatoh J, Sigrist M, Arber S, Wang F. The organization of submodality-specific touch afferent inputs in the vibrissa column. *Cell Rep* 5: 87–98, 2013.

Schnapf JL, Nunn BJ, Meister M, Baylor DA. Visual transduction in cones of the monkey Macaca fascicularis. *J Physiol* 427: 681–713, 1990.

Sherman SM. A wake-up call from the thalamus. *Nat Neurosci* 4: 344–346, 2001.

Simons DJ. Temporal and spatial integration in the rat SI vibrissa cortex. *J Neurophysiol* 54: 615–635, 1985.

Sosnik R, Haidarliu S, Ahissar E. Temporal frequency of whisker movement. I. Representations in brain stem and thalamus. *J Neurophysiol* 86: 339–353, 2001.

Viaene AN, Petrof I, Sherman SM. Synaptic properties of thalamic input to layers 2/3 and 4 of primary somatosensory and auditory cortices. *J Neurophysiol* 105: 279–292, 2011.

Wang Q, Millard DC, Zheng HJ, Stanley GB. Voltage-sensitive dye imaging reveals improved topographic activation of cortex in response to manipulation of thalamic microstimulation parameters. *J Neural Eng* 9: 26008, 2012.

Wang Q, Webber RM, Stanley GB. Thalamic synchrony and the adaptive gating of information flow to cortex. *Nat Neurosci* 13: 1534–1541, 2010.

Webber RM, Stanley GB. Nonlinear encoding of tactile patterns in the barrel cortex. *J Neurophysiol* 91: 2010–2022, 2004.

Webber RM, Stanley GB. Transient and steady-state dynamics of cortical adaptation. *J Neurophysiol* 95: 2923–2932, 2006.

Whitmire CJ, Waiblinger C, Schwarz C, Stanley GB. Information coding through adaptive gating of synchronized thalamic bursting. *Cell Rep* 14: 795–807, 2016.

Willis AM, Slater BJ, Gribkova E, Llano DA. Open-loop organization of thalamic reticular nucleus and dorsal thalamus: a computational model. *J Neurophysiol* 114: 2353–2367, 2015.

Zheng HJ, Wang Q, Stanley GB. Adaptive shaping of cortical response selectivity in the vibrissa pathway. *J Neurophysiol* 113: 3850–3865, 2015.